Flow and heat transfer of nanofluid through a horizontal microchannel with magnetic field and interfacial electrokinetic effects

Qingkai Zhao[1], Hang Xu[2], Longbin Tao[3] *

[1] College of Shipbuilding Engineering, Harbin Engineering University, Harbin 150001, China

[2] Collaborative Innovation Center for Advanced Ship and Deep-Sea Exploration (CISSE), State Key Lab of Ocean Engineering, School of Naval Architecture, Ocean and Civil Engineering, Shanghai Jiao Tong University, Shanghai 200240, China

[3] Department of Naval Architecture, Ocean and Marine Engineering, University of Strathclyde, Glasgow G4 0LZ, United Kingdom

Abstract: Flow and heat transfer of a nanofluid through a horizontal microchannel in the presence of the magnetic field effects and electric double layer (EDL) is investigated theoretically. For a microchannel with a large aspect ratio, the flow problem is treated as a two-dimensional nonlinear system. The body force generated by the EDL and magnetic field is considered in momentum equation. In order to study the mechanism of nanofluid heat transfer, the nanoparticle distribution and the heat transfer process of nanofluid flow are represented by the Buongiorno's nanofluid model with the passively controlled nanoparticle distribution at the boundary, which has not been considered in previous microchannel studies. Compared to the so-called active control of nanoparticle volume fraction at the boundary, the current approach makes the model physically more reliable by taking into account of the effect due to varying temperature. The analytical approximations obtained by the homotopy analysis method reveals that both the magnetic field effects and the EDL play significant roles on altering the flow and heat transfer in microchannels. It is also found that the heat enhancement is significantly dependent on the Brinkman number and the temperature applied to the wall.

Keywords: Nanofluid flow, Passively-controlled model, Electric double layer, Magnetic field, Microchannel

1. Introduction

With the development of miniaturization of scientific instruments, flow and heat transfer of nanofluids in micro-components have been involved in various fields, especially in medicine, aerospace and other high-tech fields [1, 2]. However,

* The corresponding author: longbin.tao@strath.ac.uk (Longbin Tao);
Email address: qkzhao@hrbeu.edu.cn (Qingkai Zhao), hangxu@sjtu.edu.cn (Hang Xu)

experimental observations [3, 4] have shown that the behaviours of fluid flow and heat transfer in a microchannel are very different from that in a macro-scale situation. Mala *et al.* [5, 6] studied the effect of the EDL on fluid flow and heat transfer in microchannel between two parallel plates. Their research shows that the EDL results in a reduced velocity of flow, thus also affects the temperature distribution. Similar conclusions and other particular features of EDL were found and studied by Ren and Li [7], You and Guo [8], Shit *et al.* [9], Jing *et al.* [10], Zhao *et al.* [11]. It was indicated that study of the flow of fluid in the micro-devices should take into account the role of the EDL.

On the other hand, magnetohydrodynamics (MHD) flow is very useful in heat and mass transfer progresses in many industrial procedures, because the applied magnetic field can affect the flow and heat transfer characteristics of the fluid [12]. Magnetic fluid is a kind of fluid containing magnetic particles, the particles of which is generally nanoscale. Therefore, magnetic fluid can be generally considered as a nanofluid and its flow and heat transfer can be theoretically studied by using nanofluid models. Recently, many researchers have paid much attention to the MHD flow and considerable effort has been devoted to experimental and theoretical research [13-17]. It is worth mentioning that Ganguly *et al.* [18] and Shit *et al.* [19] theoretically studied the electro-osmotic flow in a hydrophobic microchannel with externally applied magnetic field. Their work indicates that the magnetic field can be used to alter the distributions of velocity. Besides, Sheikholeslami and Rokni [20] analysed the flow of nanofluid convection in the presence of induced magnetic fields. The Buongiorno's nanofluid model and the active control of nanoparticle volume fraction at the boundary is adopted in their work. The results showed that the nanofluid motion reduces with the Hartmann number.

Physically, the concentration distribution of nanoparticles on the wall surface is not as easy as the temperature to be controlled. The value of the nanoparticle volume fraction at the boundary has a strong relationship with the temperature and the physical properties of nanoparticles. Kuznetsov and Nield [21] found that Brownian motion and thermophoresis have significant effects on heat transfer, and subsequently modifying the boundary conditions such that the nanoparticle volume fraction on the surface of the plate passively adjusts itself to whatever temperature is imposed on the surface of

the plate. Therefore, a passively controlled nanofluid model was proposed by Kuznetsov and Nield [22], which is more physically realistic than previous nanofluid model. Based on the passively controlled nanofluid model, Xu and Pop [23, 24] studied the flow and heat transfer of nanofluids and analysed the effects of Brownian motion and thermophoresis on the distribution of nanoparticles. It should be pointed out that the Buongiorno's nanofluid model is adopted in their work since the Buongiorno's nanofluid model can describe the relationship between temperature and nanoparticle volume fraction with coupled equations.

The aim of the present work is to investigate the flow and heat transfer of nanofluid between two horizontal plates in the presence of the magnetic field effects and EDL. The body force due to the EDL and magnetic field are taken into account in the momentum equation, meanwhile, the pressure gradient parameter is treated as unknown quantity. The energy equation and nanoparticle volume fraction equation are modelled by the Buongiorno's nanofluid model and the viscous dissipation is considered in the energy equation. As one of the highlights in the present approach, the passively controlled nanoparticles distribution is adopted at the upper plate surface. The governing equations are reduced by a set of dimensionless quantities and then solved by homotopy analysis method (HAM) [25]. The effects of the parameters of EDL and magnetic field on the velocity, temperature and nanoparticle concentration are analysed. Furthermore, the important physical quantities of practical interests are examined in detail.

2. Problem description and mathematical formulation

A pressure-driven nanofluid flow between two horizontal plates at the presence of the EDL and the externally applied magnetic field is described in the following sections. The boundary walls of the channel are held at different temperatures with the lower wall at temperature T_1 and the upper wall at temperature T_2. A passively controlled nanofluid model is adopted here and the upper plate has the passive boundary condition, while the nanoparticle volume fraction at lower plate is a constant C_1. The magnetic field of strength $\mathbf{B}$ is imposed along the *y*-axis. *L* is the length of the two plates and *H* is the distance between the two plates, as illustrated in Fig.1. The physical model and

boundary conditions in this study conform to the physical facts.

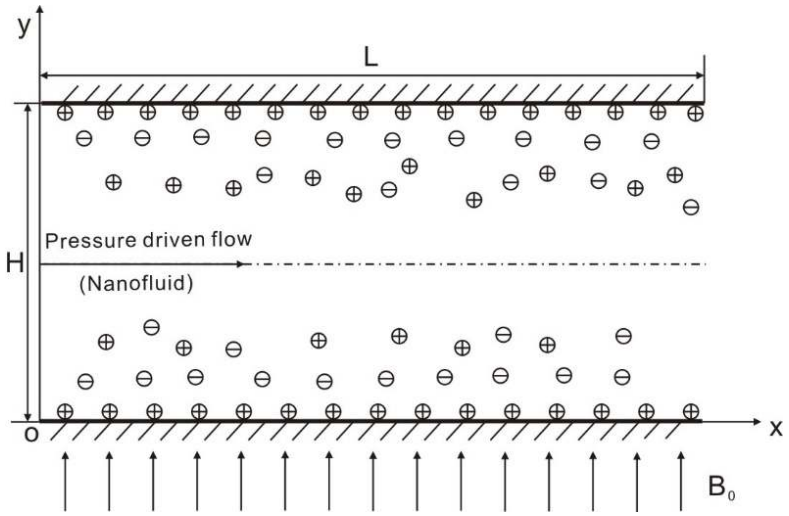

Fig1. Physical sketch of the problem.

The nanofluid flow between two horizontal plates is assumed to be steady, laminar, fully developed. Therefore, the electrostatic potential equation and Navier-Stokes equations describing the conservations of the total mass, momentum, thermal energy and nanoparticle volume fraction respectively can be written as

$$\nabla^2\psi = -\frac{\rho_e}{\varepsilon_0\varepsilon_r}, \tag{1}$$

$$\nabla\cdot\mathbf{V} = 0, \tag{2}$$

$$\rho(\mathbf{V}\cdot\nabla)\mathbf{V} = -\nabla p + \mu\nabla^2\mathbf{V} + \mathbf{F}, \tag{3}$$

$$(\mathbf{V}\cdot\nabla)T = \alpha\nabla^2 T + \tau[D_B\nabla T\cdot\nabla C + \frac{D_T}{T_0}\nabla T\cdot\nabla T] + \frac{\mu}{\rho c_p}\Phi, \tag{4}$$

$$(\mathbf{V}\cdot\nabla)C = D_B\nabla^2 C + \frac{D_T}{T_0}\nabla^2 T, \tag{5}$$

In Eqs.(1)-(5), ψ is the electrostatic potential, ε_r is the dielectric constant of the fluid, ε_0 is the permittivity of vacuum, $\mathbf{V}$ is velocity vector, ρ is the density of the fluid, μ is the viscosity, p is the pressure, $\mathbf{F} = \mathbf{E}_e\rho_e + \mathbf{J}\times\mathbf{B}$ is the body force originating from the presence of the EDL and magnetic field, $\mathbf{E}_e$ is the electric field strength generated by the electric double layer, ρ_e is the charge density, $\mathbf{J}$ is the current density vector, $\mathbf{B}$ is the magnetic flux density vector, α is the thermal diffusivity, T is the temperature, T_0 is the reference temperature, C is the

nanoparticle volume fraction, Φ is the viscous dissipation term, D_B and D_T represent the Brownian diffusion coefficient and the thermophoretic diffusion coefficient respectively, and $\tau = (\rho c_p)_p / (\rho c_p)_f$ is the heat capacity ratio. Subscripts p and f, denote the nanoparticles and the base fluid, respectively.

For parallel flow in channels, it is assumed that the velocity component of fluid is equal to zero along *y*-direction. The values of temperature and nanometer particle volume fraction in horizontal direction remain constant, namely, $\partial T/\partial x = \partial C/\partial x = 0$. The fluid thermophysical properties are held constant, and the pressure gradient is assumed to be constant. It is worth noting that the electrical force $\mathbf{E}_e \rho_e$ is caused by the EDL. Here, the direction of electric field strength is parallel to the x-axis, while the electric field strength is zero in the y-direction, namely, $\mathbf{E}_e = (E_x, 0)$. This is due to the fact that the free charged particles in the EDL surface will move along the direction of liquid flow (parallel to the x-axis), and the direction of free charge movement is parallel to the direction of electric field strength. Therefore, the electric field strength in the x direction can be noted as E_x. Similarly, the velocity of the fluid is zero in y-direction, and there is no free charge movement in y-direction. Thus, the electric field strength in the y-direction is zero. It is also assumed that the magnetic Reynolds number is small (<<1) so that the induced magnetic field can be omitted. According to Ohm's law, the current density can be written as

$$\mathbf{J} = \sigma(\mathbf{E} + \mathbf{V} \times \mathbf{B}), \tag{6}$$

where, σ is the electrical conductivity, $\mathbf{E}$ is applied electric field.

There is no applied electric field in present research, fluid motion is only owing to the pressure driven, i.e. $\mathbf{E} = 0$. In addition, $\mathbf{B} = (0, B_0)$, $\mathbf{V} = (u, 0)$. The force exerted on the fluid due to the electromagnetic interaction with the moving fluid can be written as

$$\mathbf{J} \times \mathbf{B} = \sigma(\mathbf{V} \times \mathbf{B}) \times \mathbf{B} = \sigma[\mathbf{B}(\mathbf{V} \cdot \mathbf{B}) - \mathbf{V}(\mathbf{B} \cdot \mathbf{B})] = (-\sigma B_0^2 u, 0). \tag{7}$$

Based on the above assumptions, the governing equations (1)-(5) are reduce to

$$\frac{d^2\psi}{dy^2} = -\frac{\rho_e}{\varepsilon_0 \varepsilon_r}, \tag{8}$$

$$\mu\frac{d^2u}{dy^2}-\frac{dp}{dx}-\sigma B_0^2u+E_x\rho_e=0, \tag{9}$$

$$\alpha\frac{d^2T}{dy^2}+\tau\left[D_B\frac{dT}{dy}\frac{dC}{dy}+\frac{D_T}{T_0}\left(\frac{dT}{dy}\right)^2\right]+\frac{\mu}{\rho c_p}\left(\frac{du}{dy}\right)^2=0, \tag{10}$$

$$D_B\frac{d^2C}{dy^2}+\frac{D_T}{T_0}\frac{d^2T}{dy^2}=0. \tag{11}$$

It is noted that the electric potential at the boundary between the diffuse double layer and the compact layer is zeta potential (ζ). The boundary conditions for the velocity are non-slip, which requires the x-component of the velocity to vanish at the wall. It is also assumed that the boundary conditions for the temperature are isothermal. The passive boundary condition is employed at the upper plate. With these assumptions, the appropriate boundary conditions of Eqs. (8)-(11) are

$$\psi(y)=\zeta,\ u(y)=0,\ T(y)=T_1,\ C(y)=C_1,\quad at\ \ y=0, \tag{12}$$

$$\psi(y)=\zeta,\ u(y)=0,\ T(y)=T_2,\ D_B\frac{dC}{dy}+\frac{D_T}{T_0}\frac{dT}{dy}=0,\quad at\ \ y=H. \tag{13}$$

In the channel flow research, mass flow is usually regarded as a specified quantity. Therefore, the following equation is established

$$U_m=\frac{1}{H}\int_0^H u(y)dy, \tag{14}$$

where U_m is the average velocity.

2.1 Analytical solution to the electrostatic potential

For the electrostatic potential, the relationship between ψ and ρ_e is described by the Poisson equation (8). The net charge density ρ_e in a unit volume of the fluid is given by [26]

$$\rho_e=(n^+-n^-)ze_0=-2n_0ze_0\,\mathrm{Sinh}\left(\frac{ze_0\psi}{k_b\hat{T}}\right), \tag{15}$$

where, n^+ and n^- are the number of ions of each type satisfying the Boltzmann equation $n^+=n_0\,\mathrm{Exp}(-ze_0\psi/k_b\hat{T})$ and $n^-=n_0\,\mathrm{Exp}(ze_0\psi/k_b\hat{T})$. z is the valence of

ions, e_0 is the charge of a proton, n_0 represents the bulk ionic concentration, k_b and $\hat{T}$ are the Boltzmann constant and the absolute temperature respectively.

Substituting Eq.(15) into the Poisson's equation (8), the well-known Poisson-Boltzmann equation is obtained

$$\frac{d^2\psi}{dy^2} = \frac{2n_0 z e_0}{\varepsilon_0 \varepsilon_r} \mathrm{Sinh}\left(\frac{z e_0 \psi}{k_b \hat{T}}\right). \tag{16}$$

By defining the Debye-Hückel parameter as $k = \left(2n_0 z^2 e_0^2 / \varepsilon_0 \varepsilon_r k_b \hat{T}\right)^{1/2}$, and $1/k$ is generally regarded as the EDL thickness.

Introducing the dimensionless variables

$$\eta = \frac{y}{H}, \quad \Psi(\eta) = \frac{z e_0 \psi}{k_b \hat{T}}. \tag{17}$$

Then Eq.(16) can be non-dimensionalized as

$$\frac{d^2\Psi(\eta)}{d\eta^2} = \kappa^2 \,\mathrm{Sinh}\left(\Psi(\eta)\right), \tag{18}$$

where $\kappa = Hk$.

It is assumed that the electric potential is much smaller than the thermal energy of the ions, i.e. $\left|z e_0 \psi\right| \ll \left|k_b \hat{T}\right|$. According to the Debye-Hückel linear approximation, Eq.(18) can be transformed into

$$\frac{d^2\Psi(\eta)}{d\eta^2} = \kappa^2 \Psi(\eta), \tag{19}$$

subject to the boundary conditions

$$\Psi(0) = \Psi(1) = \frac{z e_0 \zeta}{k_b \hat{T}}, \tag{20}$$

which has the analytical solution

$$\Psi(\eta) = \frac{\overline{\zeta}}{1 + e^{\kappa}} \left(e^{\kappa - \kappa\eta} + e^{\kappa\eta}\right), \tag{21}$$

where $\overline{\zeta} = z e_0 \zeta / (k_b \hat{T})$, $e^* = \exp(*)$ is exponential function.

2.2 The dimensionless form of the governing equations and boundary conditions

The streaming current is the current due to the transport of the net charge with the fluid flow. It is defined as [5]

$$I_s = \int_{\Omega} u\rho_e d\Omega , \tag{22}$$

where, Ω is the cross-sectional area of the channel, and $\Omega = H \times W$, W is the width of the plate.

The streaming potential generated by the streaming current will create an opposite current, called conduction current and is defined by

$$I_c = \lambda_0 E_x \Omega , \tag{23}$$

where, λ_0 is the electrical conductivity of the fluid, and λ_0 is assumed to be constant.

In Eq. (9), the unknown electrokinetic potential E_x can be obtained through the balance between streaming current and electrical conduction current at steady state. It means that the net electrical current should be zero at a steady state,

$$I_s + I_c = 0 . \tag{24}$$

Therefore, the electrokinetic potential E_x is obtained as

$$E_x = -\frac{1}{\lambda_0 H}\int_0^H u\rho_e dy , \tag{25}$$

Substituting Eq.(25) into Eq.(9) , the momentum equation is transformed into

$$\mu\frac{d^2u}{dy^2} - \frac{dp}{dx} - \sigma B_0^2 u - \frac{1}{\lambda_0 H}\int_0^H u\rho_e dy\rho_e = 0 . \tag{26}$$

Using Eq.(15), Eq.(17) and the Debye- Hückel linear approximation, the relationship between the net charge density ρ_e and the dimensionless electrostatic potential $\Psi(\eta)$ can be obtained as

$$\rho_e = -2n_0 z e_0 \Psi(\eta) . \tag{27}$$

Define the dimensionless quantities

$$\eta = \frac{y}{H},\ U(\eta) = \frac{u(y)}{U_m},\ \theta(\eta) = \frac{T - T_0}{T_2 - T_0},\ \phi(\eta) = \frac{C - C_0}{C_1 - C_0}, \tag{28}$$

where, C_0 is the reference nanoparticle volume fraction.

Therefore, non-dimensionalize the momentum Eq.(26) by Eq.(27) and

dimensionless quantities (28), we obtain

$$U''(\eta)+P-Ha^2U(\eta)-G\int_0^1 U(\eta)\Psi(\eta)d\eta\Psi(\eta)=0\,, \tag{29}$$

where, P is a non-dimensional parameter, Ha is the Hartmann number, G is a non-dimensional parameter and they are defined by

$$P=\frac{H^2}{\mu U_m}P_x,\ Ha=B_0H\sqrt{\frac{\sigma}{\mu}},\ G=\frac{(2n_0ze_0H)^2}{\mu\lambda_0}, \tag{30}$$

in which $P_x=-dp/dx$ is the pressure constant,

According to the boundary conditions (12), (13) and the additional boundary condition (14), the dimensionless boundary conditions for the velocity are

$$U(0)=U(1)=0,\ \int_0^1 U(\eta)d\eta=1\,, \tag{31}$$

Similarly, substituting the dimensionless quantities (28) into Eqs. (10) and (11), the reduced energy equation and volume fraction of nanoparticles equation are obtained respectively

$$\theta''(\eta)+Nb\theta'(\eta)\phi'(\eta)+Nt\theta'(\eta)^2+BrU'(\eta)^2=0\,, \tag{32}$$

$$\phi''(\eta)+\frac{Nt}{Nb}\theta''(\eta)=0\,, \tag{33}$$

the corresponding boundary conditions in non-dimensional form are

$$\theta(0)=\delta_\theta,\ \ \theta(1)=1,\ \ \phi(0)=1,\ \ Nb\phi'(1)+Nt\theta'(1)=0\,, \tag{34}$$

where, $\delta_\theta=(T_1-T_0)/(T_2-T_0)$ is constant, Br, Nb and Nt are the Brinkman number, the Brownian motion parameter and the thermophoresis parameter, respectively, and they are defined by

$$Br=Pr\cdot Ec,\ \ Nb=\frac{\tau D_B(C_1-C_0)}{\alpha},\ \ Nt=\frac{\tau D_T(T_2-T_0)}{\alpha T_0}, \tag{35}$$

in which $Pr=\nu/\alpha$ and $Ec=U_m^2/[c_p(T_2-T_0)]$ are the Prandtl number and Eckert number, respectively.

2.3 Some important physical quantities

The physically important quantities of practical interest are the skin friction, the Nusselt number and the wall mass flux. These important physical quantities are crucial to understand shear stress at the boundary, convective heat transfer and mass transfer

between the surface of two plates and the fluid flowing past it. In this case, they are defined by

$$C_{f1}=\frac{\tau_{w1}}{\frac{1}{2}\rho U_m^2}, C_{f2}=\frac{\tau_{w2}}{\frac{1}{2}\rho U_m^2}, Nu_1=\frac{Hq_{T1}}{k_f(T_1-T_0)}, Nu_2=\frac{Hq_{T2}}{k_f(T_2-T_0)},$$

$$Sh_1=\frac{Hq_{C1}}{D_B(C_1-C_0)}, Sh_2=\frac{Hq_{C2}}{D_B(C_1-C_0)}, \tag{36}$$

where,

$$\begin{aligned}&\tau_{w1}=\mu\left.\frac{du}{dy}\right|_{y=0}, \tau_{w2}=\mu\left.\frac{du}{dy}\right|_{y=H}, q_{T1}=-k_f\left.\frac{dT}{dy}\right|_{y=0}, q_{T2}=-k_f\left.\frac{dT}{dy}\right|_{y=H},\\ &q_{C1}=-D_B\left.\frac{dC}{dy}\right|_{y=0}, q_{C2}=-D_B\left.\frac{dC}{dy}\right|_{y=H}.\end{aligned} \tag{37}$$

in which, k_f is the thermal conductivity, the subscript 1 and 2 refer to the physical quantities for lower wall and upper wall, respectively.

Substituting Eqs. (28) and (37) into Eq. (36) , we obtain

$$\begin{aligned}&\mathrm{Re}\,C_{f1}=2U'(0), \mathrm{Re}\,C_{f2}=2U'(1), Nu_1=-\frac{1}{\delta_\theta}\theta'(0), Nu_2=-\theta'(1),\\ &Sh_1=-\phi'(0), Sh_2=-\phi'(1)\end{aligned} \tag{38}$$

where $\mathrm{Re}=U_m H/\nu$ is the Reynolds number,

3. Results and discussion

The non-dimensional governing equations (19), (29), (32) and (33) with the corresponding boundary conditions (20), (31) and (34) are solved for a range of values of the parameters by employing the HAM technique.

According to the HAM, the initial approximations are chosen as

$$\begin{aligned}&\Psi(0)=\eta^2-\eta+\overline{\zeta},\ U(0)=6\eta-6\eta^2,\\ &\theta(0)=\delta_\theta+(1-\delta_\theta)\eta,\ \phi(0)=\frac{Nt(\delta_\theta-1)}{Nb}\eta+1.\end{aligned} \tag{39}$$

The auxiliary linear operator are given as

$$L[\Psi(\eta)]=\frac{d^2\Psi(\eta)}{d\eta^2},\ L[U(\eta)]=\frac{d^2U(\eta)}{d\eta^2},$$
$$L[\theta(\eta)]=\frac{d^2\theta(\eta)}{d\eta^2},\ L[\phi(\eta)]=\frac{d^2\phi(\eta)}{d\eta^2}. \tag{40}$$

In the computation, the values of convergence control parameter are chosen as $\hbar_\Psi=-1/2$, $\hbar_U=-1/2$, $\hbar_\theta=-1/2$, $\hbar_\phi=-1/2$. It is worth noting that the values of the convergence control parameters can be adjusted to ensure the convergence of the results. To examine the accuracy of the results, the residual sum of square functions for the governing equations are defined as

$$\begin{aligned}
E_\Psi(m)&=\int_0^1(\Psi''-\kappa^2\Psi)^2d\eta,\\
E_U(m)&=\int_0^1(U''+P-Ha^2U-G\int_0^1U\Psi d\eta\Psi)^2d\eta,\\
E_\theta(m)&=\int_0^1(\theta''+Nb\theta'\phi'+Nt\theta'^2+BrU'^2)^2d\eta,\\
E_\phi(m)&=\int_0^1(\phi''+\frac{Nt}{Nb}\theta'')^2d\eta,
\end{aligned} \tag{41}$$

where, m is the computational order.

For instance, in the case of $\kappa=Ha=G=Br=\overline{\zeta}=1$, $Nb=0.2$, $Nt=0.1$ and $\delta_\theta=0.5$, the residual sum of squares for different orders of the solutions are obtain through the homotopy analysis method solving process (Table 1). As can be seen in Table 1, the computational errors of each equation decrease rapidly with the increase of the computational order. It is observed that the maximum residual sum of squares is 8.815×10^{-16} at 50th order HAM truncations. In order to ensure the accuracy of the results, the 50th order calculation results were adopted for analysis and discussion in present work.

Table 1. The residual sum of squares for different computational orders.

order	$E_\Psi(m)$	$E_U(m)$	$E_\theta(m)$	$E_\phi(m)$
$m=10$	2.955×10^{-7}	5.048×10^{-7}	0.334×10^{-1}	0.596×10^{-2}
$m=20$	1.538×10^{-13}	7.618×10^{-13}	8.590×10^{-6}	1.548×10^{-6}
$m=30$	1.207×10^{-19}	8.126×10^{-19}	1.820×10^{-9}	2.634×10^{-9}
$m=40$	1.032×10^{-25}	7.454×10^{-25}	1.601×10^{-12}	9.125×10^{-13}
$m=50$	8.986×10^{-32}	6.455×10^{-31}	8.815×10^{-16}	6.197×10^{-16}

Fig. 2 shows the variation trend of electric potential with different values of κ. It can be observed that the value of the electric potential decreases with the value of κ increasing. According to the definition of κ, the value of κ is inversely proportional to the thickness of the EDL. Therefore, the larger value of κ, the thinner of the thickness of the EDL, which causes the decreasing electric potential. It can be seen in Fig. 2 that the HAM solutions are in excellent agreement with the analytical solutions for $\overline{\zeta}=1$ given by Eq.(21) for different values of κ demonstrating the accuracy of the present solution.

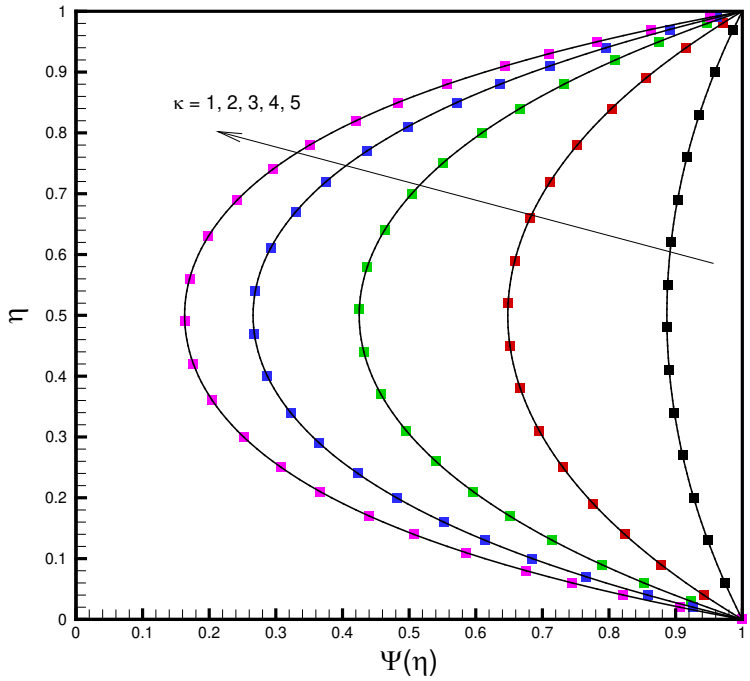

Fig.2 Comparison of the dimensionless electric potential $\Psi(\eta)$ for various values of κ with $\overline{\zeta}=1$. Line: analytical solutions given by Eq.(21); Square symbols: HAM solutions.

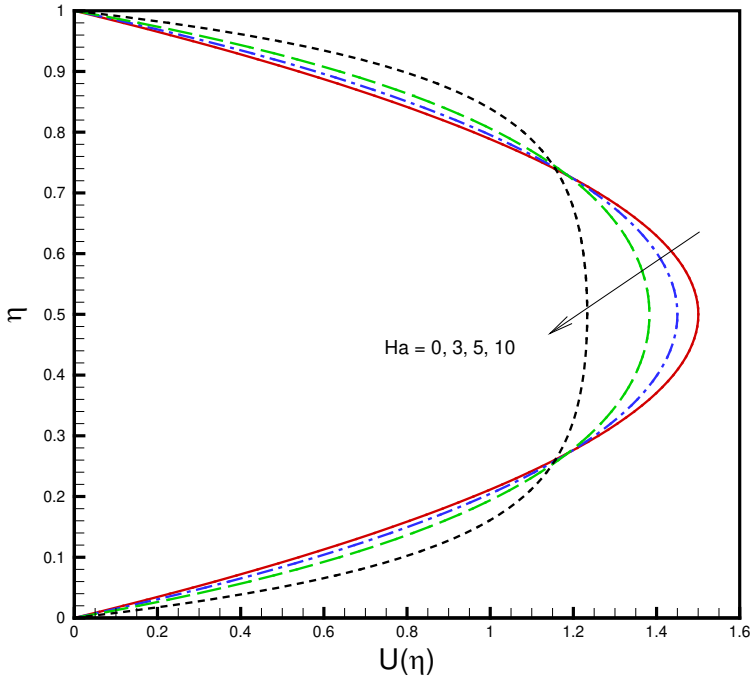

Fig.3 The dimensionless velocity profiles $U(\eta)$ for various values of Ha in the case of $Nt = 0.1, Nb = 0.2$, $\kappa = G = Br = \overline{\zeta} = 1$ and $\delta_\theta = 0.5$.

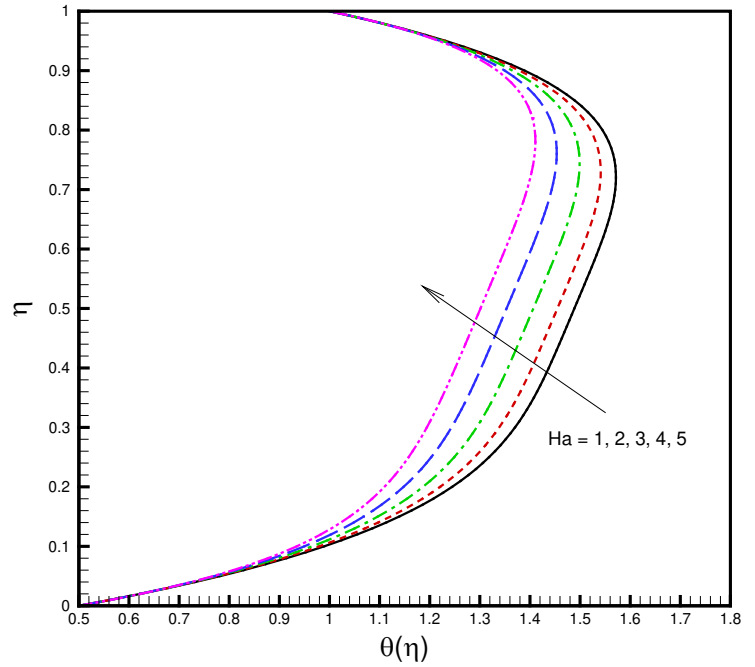

Fig.4 The dimensionless temperature profiles $\theta(\eta)$ for various values of Ha in the case of $Nt = 0.1$, $Nb = 0.2$, $\kappa = G = Br = \overline{\zeta} = 1$ and $\delta_\theta = 0.5$.

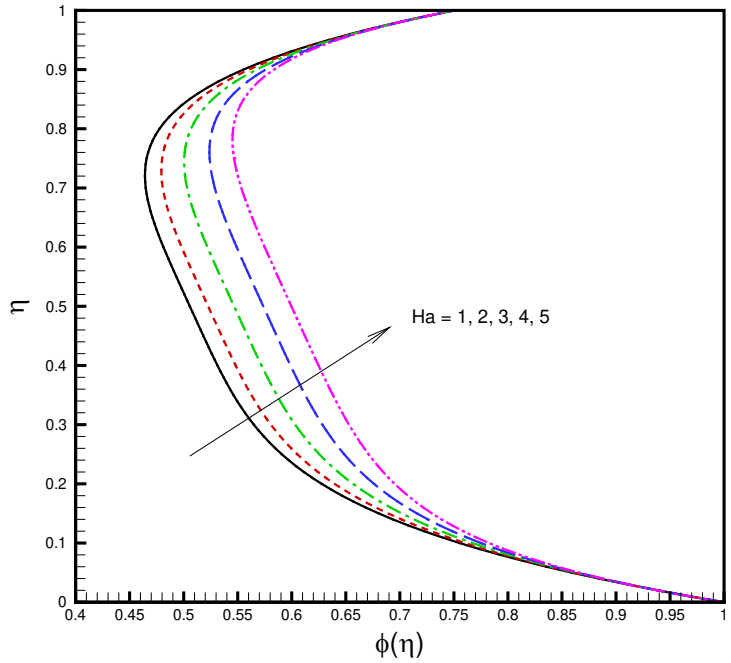

Fig.5 The nanoparticle volume fraction profiles $\phi(\eta)$ for various values of Ha in the case of $Nt = 0.1$, $Nb = 0.2$, $\kappa = G = Br = \overline{\zeta} = 1$ and $\delta_\theta = 0.5$.

The influences of Hartmann number Ha on the distribution of dimensionless velocity, temperature and nanoparticle volume fraction are shown in Fig.3, Fig.4 and Fig.5 respectively. It is shown in Fig.3 that the enlargement of the Hartmann number Ha causes slightly enhancement of the flow velocity in the vicinity of the two plates but the reduction of the flow velocity in the middle of the two plates. The impeding effect of magnetic field on flow velocity can be observed. As $Ha = 0$, namely, no magnetic field exists, the velocity distribution curve is a parabola. When $Ha \gg 1$, the magnetic field force plays an important role, and the velocity curve flattens out in the middle of the microchannel. Consequently, magnetic field slows down the flow velocity and inhibit the generation of turbulence. In Fig. 4, the dimensionless temperature profiles reduce continuously with increasing Ha due to that the enhanced Lorentz force increases the thermal boundary-layer thickness between the two plates. Unlike the dimensionless temperature, the nanoparticle volume fraction profile increases with increasing magnetic field parameter as shown in Fig. 5 as the consequence of Ha inhibiting the fluid motion, which alters the distribution of nanoparticles.

In the present work, dissipation effect in heat transfer process is considered. The Brinkman number is widely used to quantify the relationship between the heat generated by dissipation and the heat exchange at the wall. Fig.6 and Fig.7 depict the

distribution of dimensionless temperature and nanoparticle volume fraction for different Brinkman number. It is found in Fig.6 that the dimensionless temperature increases rapidly with increasing Br. On the contrary, the increase in Br reduces nanoparticle volume fraction, as shown in Fig.7. These indicate that the heat energy generated by viscous dissipation is greater than that generated by heat transfer as Br increases.

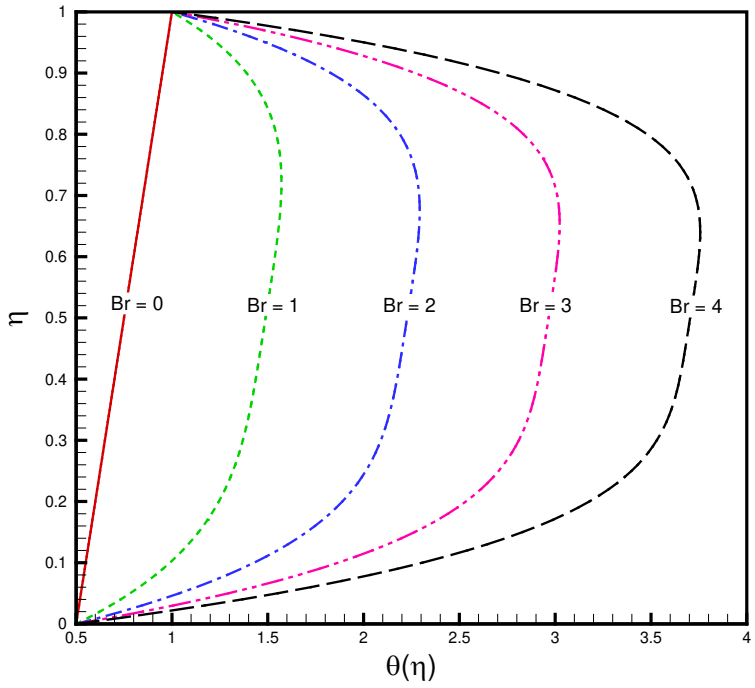

Fig.6 The dimensionless temperature profiles $\theta(\eta)$ for various values of Br in the case of $Nt = 0.1$, $Nb = 0.2$, $\kappa = G = Ha = \bar{\zeta} = 1$ and $\delta_\theta = 0.5$.

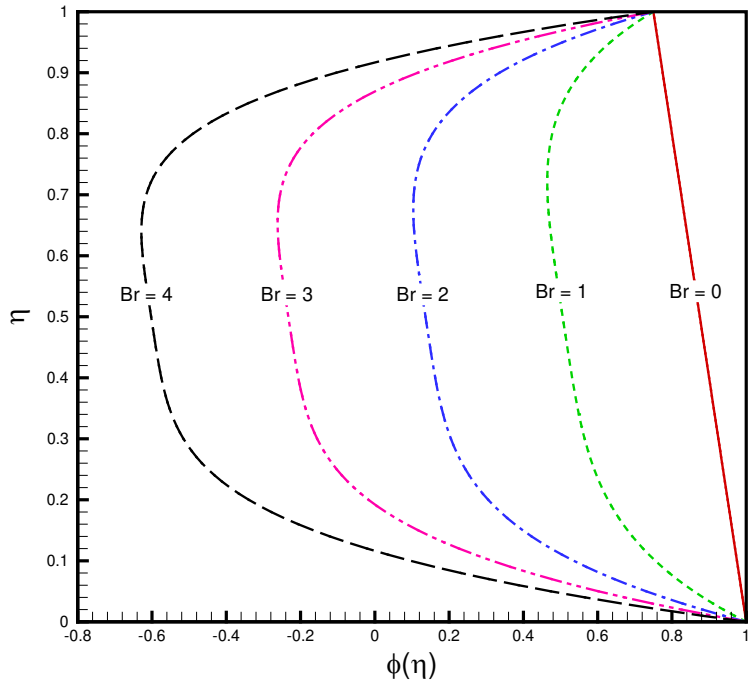

Fig.7 The nanoparticle volume fraction profiles $\phi(\eta)$ for various values of Br in the case of $Nt = 0.1$, $Nb = 0.2$, $\kappa = G = Ha = \overline{\zeta} = 1$ and $\delta_\theta = 0.5$.

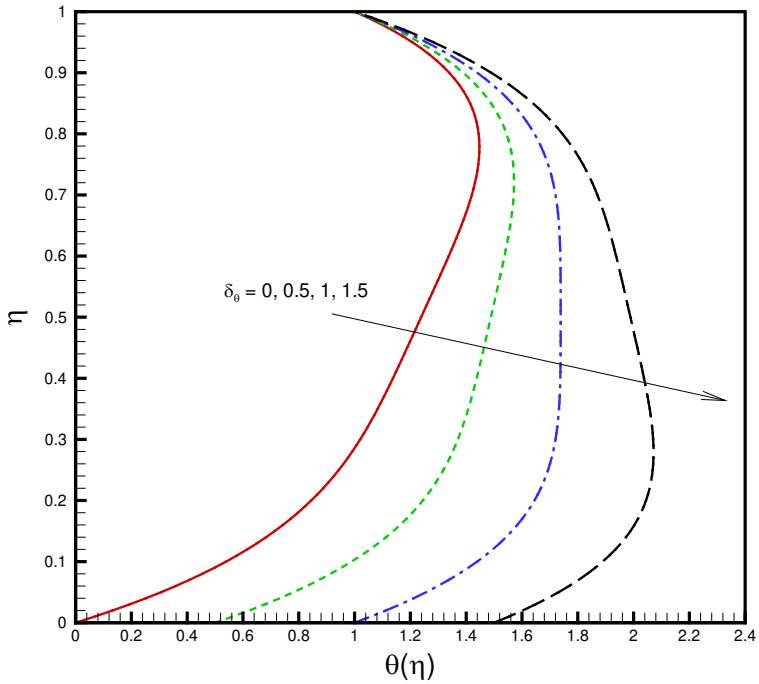

Fig.8 The dimensionless temperature profiles $\theta(\eta)$ for various values of δ_θ in the case of $Nt = 0.1$, $Nb = 0.2$, $\kappa = G = Ha = Br = \overline{\zeta} = 1$.

The influence of the lower wall temperature on the distribution of dimensionless temperature and the nanoparticle volume fraction are shown in Fig. 8 and Fig 9. It can be observed that the temperature of the lower wall has a great influence on the

temperature distribution and the nanoparticle volume fraction between the two plates. With the enhancement of the temperature on lower wall, the fluid temperature between the two plates increases considerably, as illustrated in Fig.8. Similar trend is also observed in Fig.9 where the nanoparticle volume fraction increases with the temperature on lower wall. It is a clear indication that the nanoparticle volume fraction can be controlled by the temperature of the lower wall. In order to compare the difference between active control model and passive control model, the passive control nanoparticles distribution is adopted at the upper plate surface in present work. While the nanoparticles distribution at the lower plate adopts the active control model, which makes the value of the nanoparticle volume fraction on the lower wall constant (Fig. 9). It is to be pointed out that, in reality, it is difficult to keep the nanoparticle volume fraction constant at the plate surface, especially when the temperature changes. Therefore, the passively controlled nanofluid model is more physically realistic than previous nanofluid model.

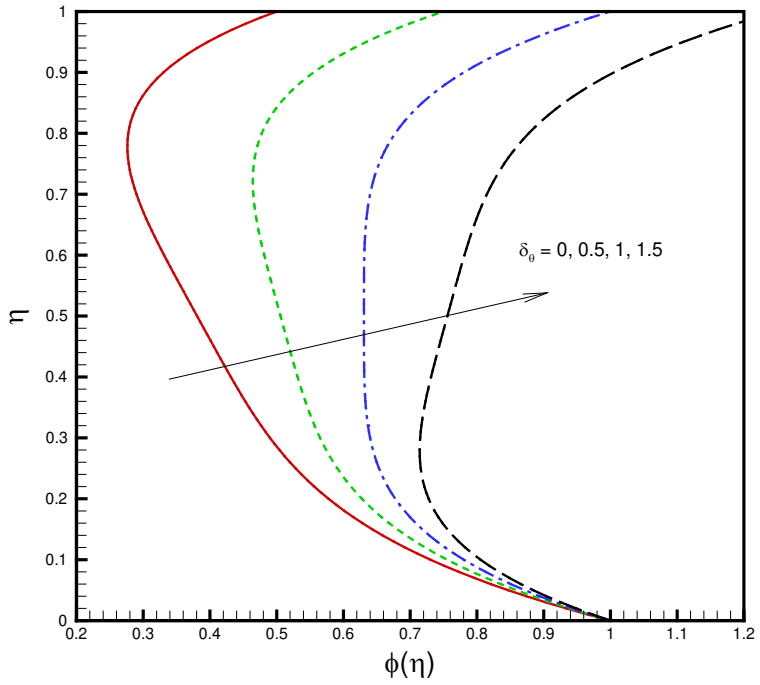

Fig.9 The nanoparticle volume fraction profiles $\phi(\eta)$ for various values of δ_θ in the case of $Nt = 0.1$, $Nb = 0.2$, $\kappa = G = Ha = Br = \overline{\zeta} = 1$.

The effects of thermophoresis parameter Nt and Brownian motion parameter Nb on the nanoparticle volume fraction are depicted in Fig.10 and Fig.11. It is seen in Fig.10 that increasing the value of the thermophoresis parameter, the nanoparticle

volume fraction decreases significantly. As observed in Fig.11, the Brownian motion parameter can alter the nanoparticle volume fraction dramatically. The enhancement of Nb leads to an increase of nanoparticle volume fraction. It is worth noting that the upper plate has the passive boundary condition due to the passively controlled nanofluid model in the present study. Therefore, the nanoparticle volume fraction on the upper wall varies with the change of Nt and Nb. This behaviour agrees with the studies of Kuznetsov and Nield [22].

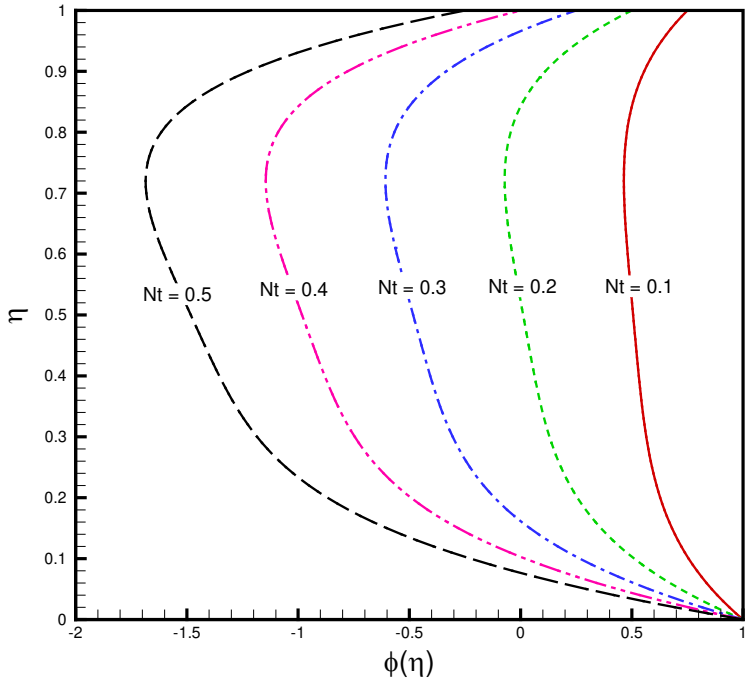

Fig.10 The nanoparticle volume fraction profiles $\phi(\eta)$ for various values of Nt in the case of $Nb = 0.2$, $\kappa = G = Ha = Br = \overline{\zeta} = 1$ and $\delta_\theta = 0.5$.

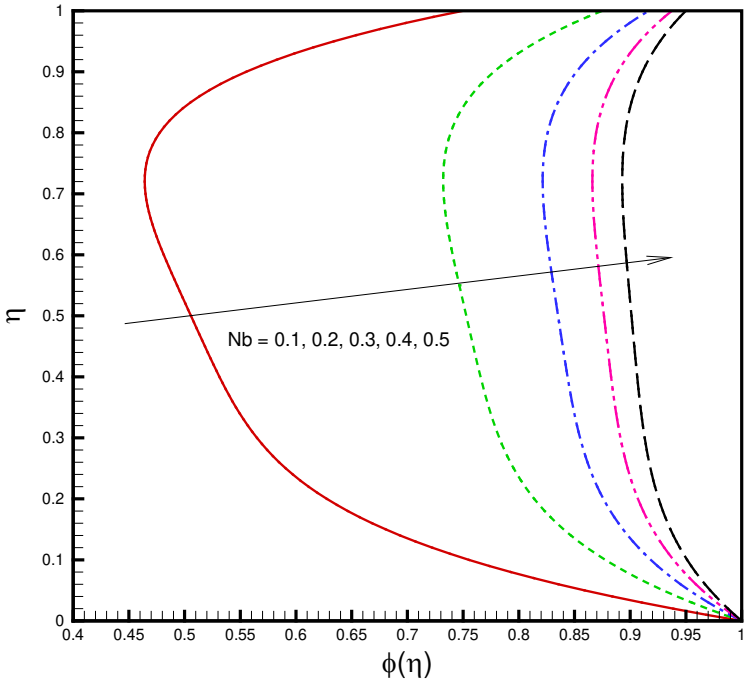

Fig.11 The nanoparticle volume fraction profiles $\phi(\eta)$ for various values of Nb in the case of $Nt = 0.1$, $\kappa = G = Ha = Br = \overline{\zeta} = 1$ and $\delta_\theta = 0.5$.

The effect of κ on the pressure constant P with different values of Ha is shown in Fig.12. It is seen that the pressure constant decreases monotonously as κ increases. When κ is sufficiently large, the pressure constant approaches to a constant value. As the value of κ increases, the thickness of EDL reduces, which leads to a weakening of the EDL effect. The strong EDL can lead to back flow near the channel wall which induces a stronger flow resistance in the bulk fluid. Therefore, when κ is sufficiently large, the flow resistance caused by the EDL can be neglected, and the velocity of the fluid increases. It is worth mentioning that the variation trend of the pressure constant is consistent with the result of previous study [11]. Different from the previous study, however, both the EDL and the magnetic field effects are considered in present work. The variation of the pressure constant P with the Hartmann number Ha is also illustrated in Fig.12. It is found that the Hartmann number has a significant effect on the pressure constant. The increase of Ha leads to a rapid enhancement of the pressure constant.

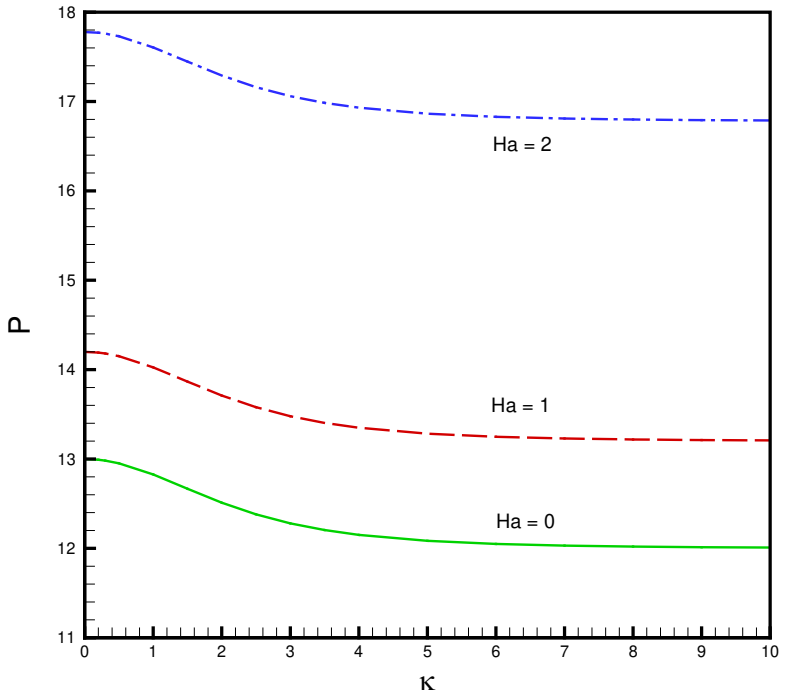

Fig.12 Variation of the pressure constant P with κ in the case of $Nt = 0.1$, $Nb = 0.2$, $G = Br = \overline{\zeta} = 1$ and $\delta_\theta = 0.5$.

Many studies on nanofluid flow containing the magnetic field effect have been reported, however, the effects of magnetic field on friction coefficient, Nusselt number and Sherwood number are seldom studied. Thus, the influence of Hartmann number on these physical quantities are examined in detail. It can be seen in Fig.13 that the variation of Ha causes the different trends for these physical quantities. The increase of Ha leads to a slight increase of the skin friction on the upper wall, but results in the decrease slightly of the skin friction on the lower wall. It is also observed that the effects of magnetic field parameter on Nusselt number and Sherwood number are negligible. However, the influence of the Hartmann number on the pressure parameter is significant. The pressure parameter P increases monotonically as Ha increases. According to Bernoulli's principle, the velocity decreases with increasing pressure. Therefore, increasing the magnetic field has the effect of inhibiting the flow rate, which is consistent with the finding shown in Fig.3.

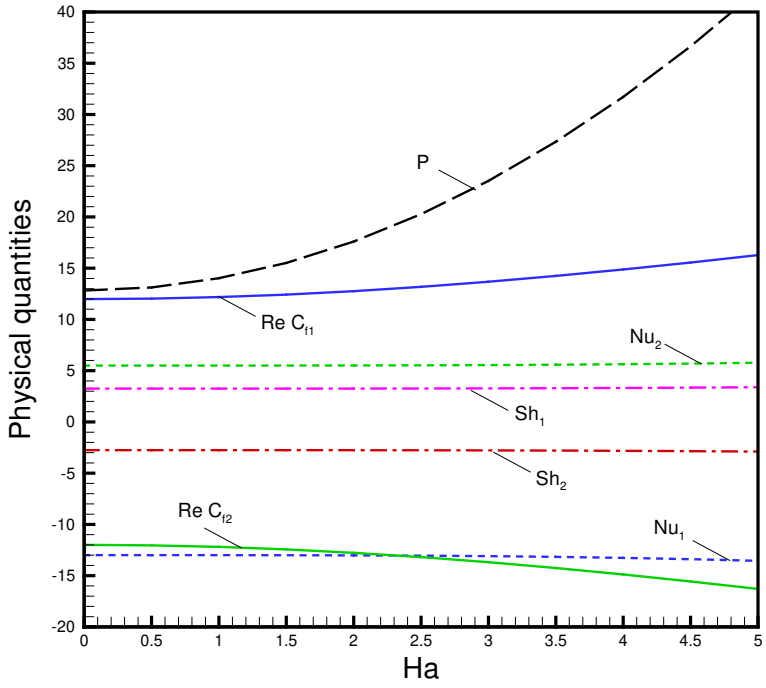

Fig.13 Variation of the physical quantities with Ha in the case of $Nt = 0.1$, $Nb = 0.2$, $\kappa = G = Br = \overline{\zeta} = 1$ and $\delta_\theta = 0.5$.

4. Conclusions

The behaviour of nanofluid flow and heat transfer between two horizontal plates considering the magnetic field effects and EDL is investigated in this paper. The passively controlled mathematical model for nanofluids is employed. In addition, the pressure gradient parameter is treated as unknown quantity and the viscous dissipation is considered in energy equation. The improved model with consideration of these conditions represents more physical reality of the problem. By using the HAM solution technique, the effect of the parameter κ, the Hartmann number Ha, the Brinkman number Br, the lower wall temperature δ_θ, the thermophoresis parameter Nt and the Brownian motion parameter Nb on the dimensionless electric potential, velocity, temperature, nanoparticle volume fraction and various physical quantities are examined and discussed in detail. The results revealed that the magnetic field and EDL can be used to control the flow and heat transfer in microchannels. It is also found that the heat enhancement is significantly depend on the Brinkman number and the temperature applied to the wall. In addition, the magnetic field has an effect on the nanoparticle volume fraction and the friction coefficient, however the effect of the magnetic field on

Nusselt number and Sherwood number can be neglected in present problem. These findings provide important guidance for the application of microfluidic devices under the external applied magnetic field.

Acknowledgement

This research is supported by China Postdoctoral Science Foundation funded project (Grant NO.2018M631909) and Heilongjiang Postdoctoral Grant (LBH-Z18059).

Reference

[1] Sidik N A C, Samion S, Ghaderian J. Recent progress on the application of nanofluids in minimum quantity lubrication machining: A review. International Journal of Heat and Mass Transfer, 2017, 108:79-89.

[2] Gupta M, Singh V, Kumar R, Said Z. A review on thermophysical properties of nanofluids and heat transfer applications. Renewable and Sustainable Energy Reviews, 2017, 74(2):638-670.

[3] Peng X F, Peterson G P, Wang B X. Heat transfer characteristics of water flowing through microchannels. Experimental Heat Transfer, 1994, 7(4), 265-283.

[4] Wang B X, Peng X F. Experimental investigation on liquid forced-convection heat transfer through microchannels. International Journal of Heat and Mass Transfer, 1994, 37:73-82.

[5] Mala G M, Li D, Werner C, Jacobash H J, Ning Y B. Flow characteristics of water through a microchannel between two parallel plates with electrokinetic effects. International Journal of Heat and Fluid Flow, 1997, 18(5):489-496.

[6] Mala G M, Li D, Dale J D. Heat transfer and fluid flow in microchannels. International Journal of Heat and Mass Transfer, 1997, 40(13):3079-3088.

[7] Ren C L, Li D. Improved understanding of the effect of electrical double layer on pressure-driven flow in microchannels. Analytica Chimica Acta, 2005, 531(1):15-23.

[8] You X Y, Guo L. Combined effects of EDL and boundary slip on mean flow and its stability in microchannels. Comptes Rendus Mecanique, 2010, 338(4):181-190.

[9] Shit G C, Mondal A, Sinha A, Kundu P K. Two-layer electro-osmotic flow and heat transfer in a hydrophobic microchannel with fluid-solid interfacial slip and zeta potential difference. Colloids and Surfaces A: Physicochemical and Engineering Aspects, 2016: S0927775716305039.

[10] Jing D, Pan Y, Wang X. The non-monotonic overlapping EDL-induced electroviscous effect with surface charge-dependent slip and its size dependence.

International Journal of Heat and Mass Transfer, 2017, 113:32-39.
[11] Zhao Q, Xu H, Tao L. Nanofluid flow and heat transfer in a microchannel with interfacial electrokinetic effects. International Journal of Heat and Mass Transfer, 2018, 124:158-167.
[12] Nkurikiyimfura I, Wang Y, Pan Z. Heat transfer enhancement by magnetic nanofluids—A review. Renewable and Sustainable Energy Reviews, 2013, 21:548-561.
[13] Attia H A. Unsteady MHD flow and heat transfer of dusty fluid between parallel plates with variable physical properties. Applied Mathematical Modelling, 2002, 26(9):863-875.
[14] Zeeshan A, Ellahi R, Hassan M. Magnetohydrodynamic flow of water/ethylene glycol based nanofluids with natural convection through a porous medium. The European Physical Journal Plus, 2014, 129(12):261.
[15] Sheikholeslami M, Hatami M, Ganji D D. Nanofluid flow and heat transfer in a rotating system in the presence of a magnetic field. Journal of Molecular Liquids, 2014, 190(190):112-120.
[16] Fakour M, Vahabzadeh A, Ganji D D. Study of heat transfer and flow of nanofluid in permeable channel in the presence of magnetic field. Propulsion and Power Research, 2015, 4(1):50-62.
[17] Hatami N, Banari A K, Malekzadeh A, Pouranfard A R. The effect of magnetic field on nanofluids heat transfer through a uniformly heated horizontal tube. Physics Letters A, 2017, 381(5):510-515.
[18] Ganguly S, Sarkar S, Hota T K, Mishra M. Thermally developing combined electroosmotic and pressure-driven flow of nanofluids in a microchannel under the effect of magnetic field. Chemical Engineering Science, 2015, 126(April):10-21.
[19] Shit G C, Mondal A, Sinha A, Kundu P K. Electro-osmotically driven MHD flow and heat transfer in microchannel. Physica A: Statistical Mechanics and its Applications, 2016, 449:S0378437116000169.
[20] Sheikholeslami M, Rokni H B. Nanofluid two phase model analysis in existence of induced magnetic field. International Journal of Heat and Mass Transfer, 2017, 107:288-299.
[21] Kuznetsov A V, Nield D A. Natural convective boundary-layer flow of a nanofluid past a vertical plate. International Journal of Thermal Sciences, 2010, 49(2):243-247.
[22] Kuznetsov A V, Nield D A. The Cheng-Minkowycz problem for natural convective boundary layer flow in a porous medium saturated by a nanofluid: A revised model. International Journal of Heat and Mass Transfer, 2013, 65(1-3):682-685.
[23] Xu H, Pop I. Mixed convection flow of a nanofluid over a stretching surface with uniform free stream in the presence of both nanoparticles and gyrotactic microorganisms. International Journal of Heat and Mass Transfer, 2014, 75:610-623.
[24] Xu H, Pop I. Fully developed mixed convection flow in a horizontal channel filled by a nanofluid containing both nanoparticles and gyrotactic microorganisms. European Journal of Mechanics, 2014, 46(12):37-45.

[25] Liao S J. Homotopy Analysis Method in Nonlinear Differential Equations, Higher Education Press, Beijing, 2012.
[26] Hunter R J. Zeta Potential in Colloid Science, Principles and Applications, Academic Press, New York, 1981.